

# Parameter Estimation of a DOC from Engine Rig Experiments with a Discretized Catalyst Washcoat Model

Björn Lundberg  
Chalmers Univ. of Technology

Jonas Sjoblom  
Chalmers Univ of Technology

Åsa Johansson  
Johnson Matthey ECT

Björn Westerberg  
Scania AB

Derek Creaser  
Chalmers Univ of Technology

## ABSTRACT

Parameter tuning was performed against data from a full scale engine rig with a Diesel Oxidation Catalysts (DOC). Several different catalyst configurations were used with varying Pt loading, washcoat thickness and volume. To illustrate the interplay between kinetics and mass transport, engine operating points were chosen with a wide variation in variables (inlet conditions) and both transient and stationary operation was used. A catalyst model was developed where the catalyst washcoat was discretized as tanks in series both radially and axially. Three different model configurations were used for parameter tuning, evaluating three different approaches to modeling of internal transport resistance. It was concluded that for a catalyst model with internal transport resistance the best fit could be achieved if some parameters affecting the internal mass transport were tuned in addition to the kinetic parameters. However it was also shown that a model with negligible internal transport resistance still could obtain a good fit since kinetic parameters could compensate for transport limitations. This highlighted the inherent difficulties using kinetic models with high parameter correlation and also showed the importance of using a kinetic model with a structure that is capable of describing exclusively intrinsic kinetics.

**CITATION:** Lundberg, B., Sjoblom, J., Johansson, Å., Westerberg, B. et al., "Parameter Estimation of a DOC from Engine Rig Experiments with a Discretized Catalyst Washcoat Model," *SAE Int. J. Engines* 7(2):2014, doi:10.4271/2014-01-9049.

---

## INTRODUCTION

The diesel oxidation catalyst (DOC) is a well established technology to reduce CO and hydrocarbon (HC) emissions from diesel engines that has been in use since the 1990s. Strengthened emission standards have made the importance of the DOC even greater in recent years since it has become an indispensable part in enhancing the performance of diesel particulate filters (DPF) and selective catalytic reduction (SCR) by utilization of oxidation of NO to NO<sub>2</sub>. Therefore a correct prediction of the performance of the DOC is very important for the simulation of the entire aftertreatment system.

A vital part of parameter estimation is the formulation of the catalyst model that will be used in the simulations. The model does not only need an accurate description of the reactions taking place in the washcoat but the transport of reacting components from the gas bulk to the washcoat is also of greatest importance. A phenomenon that is very rarely taken into consideration when full scale DOC systems are modeled, but is more common for SCR [1] and Ammonia Slip Catalysts (ASC) [2], is the pore transport resistance. Studies at lab scale have, however, shown that it indeed can be of influence for the conversion of HC [3], CO [3, 4] as well as NO [5].

Large efforts have been made to construct kinetic models for the DOC both of global type [6, 7, 8, 9] and microkinetic type [10, 11, 12]. Kinetic models used for full-scale simulations are in most cases of global type. Since the global kinetic models derived from full-scale simulations generally have been fitted to data in which both transport and reaction rate limited conditions prevail, there is a risk that the resulting kinetic parameters are not purely intrinsic. This means that varying physical properties of the catalyst (such as washcoat thickness, pore size distribution, noble metal loading and other ageing effects) tends to make the kinetic parameters case specific, resulting in the kinetic model only giving reliable predictions for a catalyst close to the one used in the experiments from which the model was derived [13]. A method of retuning parameters to measurement data where catalyst physical properties are efficiently separated from kinetics is therefore desirable. To make such separation possible a model with enough complexity to accurately describe the mass transfer in the washcoat and at the gas-washcoat interface is vital.

In order to evaluate the importance of pore transport resistance or create models that accurately account for it, the effective diffusivities must be known. Effective diffusivities may be calculated from models of varying sophistication which require knowledge of the physical properties of the catalysts [14] and in some cases the detailed pore structure [15, 16]. Still these calculated effective diffusivities can only be regarded as initial estimates, especially considering that they would in the case of hydrocarbons in an exhaust gas, likely be based on a single model species. Alternatively, it is possible to make direct experimental measurements of the effective diffusivity with actual monolith structures by for example chromatographic techniques [17] or in the form of a Wicke Kallenbach diffusion cell [18]. However, these approaches require specialized equipment and again measurements would undoubtedly have to be carried out under conditions that differ somewhat from a true exhaust gas.

The advantage of using an engine-rig is that parameters are estimated directly for their purpose, i.e. full-scale simulations, but the drawback is increased experimental time and the fact that the feed gas composition and resulting experimental space is limited to what is possible for the engine to produce. These engine limitations coupled with the importance of obtaining pertinent experimental data that aids in the distinction between kinetic and transport effects makes a good experimental design very important.

In the current study we present and evaluate an approach where effective diffusivities are fine-tuned in parallel with the estimation of kinetic parameters from experiments with actual exhaust gas generated by an engine. In comparison, two additional models were created where only kinetic parameters were tuned and effective diffusivities remained constant. For one of these models internal transport resistance was neglected. The resulting tuned kinetic models were compared in an effort to investigate the effect of modeling of internal transport resistance. The study also includes Design of

Experiments (DoE) to generate a manageable transient data set that effectively spans the complete operating conditions of the engine and reduces the high correlation between variables that is characteristic for a full scale system. To further enhance the separation of kinetic and transport effects different catalyst configurations with varying Pt loading, washcoat thickness and volume were included in the experimental plan.

## EXPERIMENTAL SECTION

All experiments in the present work were performed with a full scale engine rig which also means that the catalysts used were all of dimensions for heavy-duty vehicle aftertreatment systems. The catalysts were of monolith flow-through type with a total diameter of 30.5 cm (12 inch) and a length of 10.2 cm (4 inch). The active material, platinum, was dispersed in a washcoat distributed on the channel walls which means that the reacting species needed to diffuse through the washcoat to react on the active sites. Using an engine as the exhaust source together with full scale catalysts results in challenges for achieving proper design of experiments, catalyst model formulation, and parameter tuning. All of these issues as well as how they were handled in this study are presented in this section.

### The Reactor Model

A full scale catalyst monolith, connected to an engine with varying inlet properties displays a highly dynamic behavior. This means that the catalyst outlet conditions will not only be influenced by the current inlet conditions but also those at previous time points. To describe this behavior a transient catalytic reactor model is needed. In this work a uniform radial flow and concentration distribution over the catalyst cross section was assumed which makes it sufficient to model only one channel. The single channel model, closely based on the model presented by Ericson et al. [19], was discretized as tanks in series where the catalyst washcoat was discretized both radially and axially while the gas phase was only discretized axially. This 1D/2D (gas phase/washcoat) structure was chosen since it was considered a good compromise between accuracy and computational speed [20]. A film theory model was used to model the heat and mass transport between gas and washcoat surface. Axial diffusion and radial temperature gradients in the washcoat were neglected.

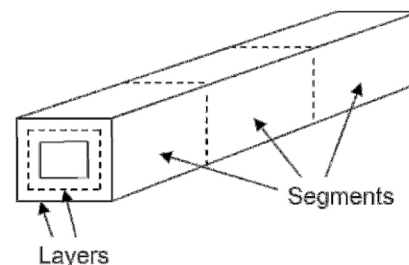


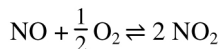
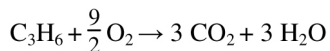
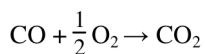
Figure 1. Illustration of the catalyst discretization principle demonstrated by a single channel.

The wide temperature range of vehicle exhaust together with the need to package as much activity into a given volume of the converter as possible to achieve vehicle on-board space-efficiency, leads to transport limitations usually becoming unavoidable at higher temperature. This means that significant gradients in the washcoat are likely to occur which makes the washcoat discretization specifically important for a proper description of the behavior of the system. Full-scale experiments also mean that some additional properties that might be negligible for lab-scale, such as heat losses and heat accumulation in pipes and canning, needed to be included (or taken into account) in the reactor model. A thorough description of the catalyst model is given in the [appendix](#).

## Kinetics

The simplest versions of the DOC kinetic models only describe the oxidation reactions of CO, hydrocarbons (HC) and NO. In addition HC is often represented as one molecular species, usually propene [6, 13, 21]. The exhaust composition is far more complex than just one type of hydrocarbon species and there are examples of kinetic models [8, 22] that have been expanded with several types of HC. Other additional reactions that may be added are H<sub>2</sub> oxidation [12, 22] and HC oxidation by NO [7, 23] or by NO<sub>2</sub> [8]. In this work rather than focusing on the required model formulation or level of detail of the kinetic model, it was the method used to estimate kinetic parameters for a given kinetic model that was in focus.

The kinetic model used in this study is of Langmuir-Hinshelwood type and was originally suggested in the classical work by Voltz et al [6] and later modified by Oh and Cavendish [21]. The model, which has been widely and frequently used in DOC modeling over the years, only includes three reactions of which one is an equilibrium reaction:



The reaction rates were calculated according to [equation 1, 2, 3, 4, 5](#).

$$r_1 = \frac{k_1 y_{\text{CO}} y_{\text{O}_2}}{G(y_i, T_s)} \quad (1)$$

$$r_2 = \frac{k_2 y_{\text{C}_3\text{H}_6} y_{\text{O}_2}}{G(y_i, T_s)} \quad (2)$$

$$r_3 = \frac{k_3 y_{\text{NO}} y_{\text{O}_2}}{G(y_i, T_s)} \left( 1 - \frac{K'}{K_p} \right) \quad (3)$$

$$K' = \frac{y_{\text{NO}_2}}{y_{\text{NO}} y_{\text{O}_2}^{1/2}} \quad (4)$$

$$G(y_i, T_s) = T_s \left( 1 + K_4 y_{\text{CO}} + K_5 y_{\text{C}_3\text{H}_6} \right)^2 \left( 1 + K_6 y_{\text{CO}}^2 y_{\text{C}_3\text{H}_6}^2 \right) \left( 1 + K_7 y_{\text{NO}}^{0.7} \right) \quad (5)$$

Where  $K_j$  is the reaction rate coefficient for the inhibition terms in the denominator  $G$  and  $K_p$  is the equilibrium constant for NO oxidation. At thermodynamic equilibrium,  $K_p$  will be equal to  $K'$  and reaction rate  $r_3$  will be equal to zero. Both reaction rate coefficients  $k_j$  and  $K_j$  were described by Arrhenius expressions:

$$k_j = A_j e^{-\frac{E_{A,j}}{RT_s}} \quad (6)$$

The start values for estimation of kinetic parameters were taken from [13] where results from several studies [24, 25, 26, 27, 28, 29, 30] were compiled. The initial values for kinetic parameter estimation used in this study are shown in [table 6](#).

The kinetic parameters in [equations 1, 2, 3, 4, 5](#) are in some cases highly correlated and since the initial parameter values in [table 6](#) were taken from different studies, the fit of the model to experimental data was expected to be poor before any parameter tuning was performed. However, the parameters were successfully used as a starting point for parameter tuning of a DOC against engine rig data in [13] which was also the intended application in the present work.

## Adjustable Parameters

To tune the model to the measurement data a number of parameters in scaled and centered forms [31] can be adjusted. These parameters can be divided into kinetic parameters, mass transfer parameters and heat transfer parameters. In the current section some extra attention will be given to the mass transfer parameters and some of the kinetic parameters, all the adjustable parameters are however described in detail in the [appendix](#).

## Kinetic Parameters

Three types of kinetic parameters are adjusted; pre-exponential factors, activation energies and activity scaling factors. The former two are described in the [appendix](#).

It has been shown that the catalyst active surface area could be used as a single parameter in a global model [32]. In addition to the pre-exponential factors and the activation energies, an activity scaling factor has therefore also been selected as an adjustable kinetic parameter. The activity scaling factor is simply a scale factor for all reaction rates on a certain site on a certain catalyst (parameters were tuned to several different catalysts simultaneously) with the purpose of

accounting for different properties of catalyst samples, such as metal dispersion. This means that the catalyst active surface area ( $A_m$ ) was tuned for each catalyst sample since only one single site is used in the kinetic model.

### Mass Transfer Parameters

The species used in the kinetic model are  $O_2$ , NO,  $NO_2$ , CO, and HC which means that these also are the species whose mass transport is significant for the behavior of the model. In the current study the effective diffusivity was initially calculated as a function of the  $f_D$  factor, the gas diffusivity and the Knudsen diffusivity according to [equation A13](#) in the appendix. This expression is only an estimate of the transport resistance in the complex porous body that is a catalyst washcoat. Firstly the  $f_D$  factor itself should account for both the tortuosity and the porosity by just one constant which makes it difficult to estimate. Secondly the structure of the pores may contain cracks and other discrepancies which would make the resistances in parallel suggested by the model (denominator of  $1/D_{i,k} + 1/DK_{i,k}$  in [equation A13](#)) far from reality. Tuning the effective diffusivities was therefore evaluated as a method of tuning the transport resistance with the aim of reducing the correlation between mass transport and kinetic parameters.

The species were divided into two groups, where the first group contained  $O_2$ , NO,  $NO_2$ , and CO and the second group contained HC. In the first group all species are well defined with similar diffusivities and could be expected to have similar mass transport properties in the washcoat with presumably the same bias from their true values. To reduce the number of parameters to tune the same scale factor was used for all species in this group. The second group contained HC which was represented as  $C_3H_6$  but in reality it is a wide range of hydrocarbons with different mass transport properties. The scale factor for the second group was in other words expected to be influenced both by the hydrocarbon composition and the washcoat structure while the scale factor for the first group mainly accounted for only washcoat structure. The equations for adjusting the mass transfer parameters can be found in in the [appendix](#).

## Experimental Set-up

### Engine Rig

A Euro IV calibrated heavy duty diesel engine with disabled exhaust gas recirculation (EGR) was used as the exhaust source and Swedish MK1 diesel, a commercial low-sulfur (approximately 5 ppm S) diesel, was used as fuel. The engine was equipped with a dynamometer control system enabling independent control of load and speed. A change in operating point for the engine could be implemented very fast, although the dynamics of the engine rig itself were much slower due to the large thermal mass.

### Catalysts

To further widen the experimental range, four different catalyst configurations with different noble metal loading, lengths, and washcoat thicknesses were used. All catalysts, shown in [table 1](#), were Pt on alumina model catalysts provided by Johnson Matthey.

**Table 1.** Catalyst configuration used for parameter estimation (a-d). Catalyst configuration c consists of two catalysts in series. The Pt-loading is shown in both mass % of washcoat and  $g/ft^3$  total catalyst volume.

<u>Config- uration</u>	<u>Pt- loading</u> [mass % washcoat]	<u>Pt-loading</u> [ $g/ft^3$ mon- olith]	<u>Length</u> [cm]	<u>Washcoat thickness</u> [mm]
<b>a</b>	0.30	15	10.2	0.110
<b>b</b>	0.59	30	10.2	0.110
<b>c</b>	0.30	15	2x10.2	0.110
<b>d</b>	0.59	15	10.2	0.055

All configurations have a 30.5 cm diameter (12 inch), 62 channels/cm<sup>2</sup> (400 cpsi) cell density and a wall thickness of 0.152 mm and the substrate material used was cordierite. The catalysts were thermally aged for one hour at 600°C.

### Measurements

The temperature and composition measurements were made according to [figure 2](#) where the downstream catalyst position (Cat. 2) is left empty for all configurations except configuration c (see [table 1](#)).

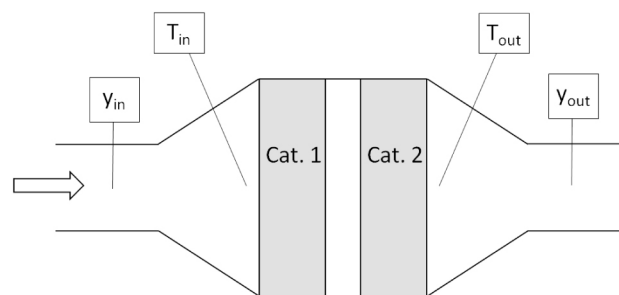


**Figure 2.** Illustration of temperature and gas composition measurement

The temperatures were measured with 3 mm thermocouples positioned at the center of the pipe and close to the catalysts. The inlet gas composition was measured just before the pipe expansion and the outlet gas composition was measured directly downstream the pipe contraction. Separate analyzer units were used to measure the concentration of CO (infra-red),  $CO_2$  (infra-red), NO and  $NO_x$  (chemiluminescence), total hydrocarbon (flame ionization) and  $O_2$  (electrochemical cell). The  $NO_2$  composition was determined by the  $NO_x$  and NO difference. Although measurements of total hydrocarbon were made, results here will be reported as equivalent concentrations of the selected model hydrocarbon compound, propene ( $C_3H_6$ ). The total mass flow into the catalyst is

calculated from the sum of the air mass flow and the fuel flow to the engine. The air mass flow was measured using a thermal mass flow meter and the fuel flow is measured using a continuous fuel meter

Since the flow resistance will depend on the catalyst length an orifice was used to maintain constant engine out back pressure independent of the catalyst configuration. This was done to ensure that a certain engine load and speed would generate the same exhaust composition and flow for all configurations. The pressure in the catalyst was near atmospheric which was assumed when concentration calculations were performed with the ideal gas law.

### Parameter Estimation Method

As mentioned in the introduction the available exhaust composition, flow and temperature is limited by the operating points of the engine. It also takes several minutes for the catalyst inlet conditions to reach stability when switching between operating points, which means that experimental time will be a factor when deciding the number of different operating points when the full transient behavior is of interest. An important part of the current work is to investigate what experiments are suitable for parameter tuning and therefore both transient and steady-state data is desirable. Since the number of catalyst configurations was large (table 1) and some replicates also were necessary only 8 different operating points were selected according to table 2. The variables in the table have the following approximate spans;  $\text{NO}_x$  100-1600 ppm, HC 50-200 ppm, CO 0-200 ppm,  $\text{O}_2$  5-20 %, temperature 200-500°C and flow 5-40 kg/s. The operating points were selected manually but were later confirmed to be a close to D-optimal selection with a model based design analysis of the engine map in temperature, concentrations and flow. Figure 3 shows an example of how the operating points span over the engine map for the case of temperature.

Table 2. Engine operation points and levels of variables, Med=medium.

Number	Description				
	$\text{NO}_x$	HC + CO	$\text{O}_2$	Temp.	Flow
1	Low	High	High	Low	Low
2	Low	High	High	Low	Med
3	High	Med	Med	Med	Low
4	Med	Low	Med	Med	High
5	High	Low	Low	High	Med
6	Med	Low	Med	Med	High
7	High	Low	Low	High	Med
8	Med	Low	Low	High	High

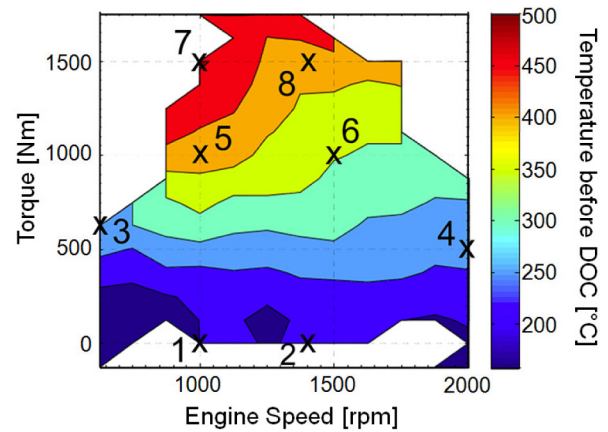


Figure 3. Temperature engine map and selected operating points

The operating points were selected to make as large steps as possible in the different variables including concentrations of  $\text{NO}$ ,  $\text{NO}_2$ , HC, CO and  $\text{O}_2$  as well as temperature and flow rate with the purpose of making the experimental space as large as possible. Some of the variables, such as concentrations of  $\text{NO}$  and  $\text{NO}_2$  and concentrations of HC and CO, are closely correlated and it is difficult to create transients where they are changed independently. This is also the case for  $\text{O}_2$  and temperature, i.e. an operation point with low temperature will have high oxygen concentration and an operation point with high temperature will have low oxygen concentration. This means that some of the input variables cannot be varied independently. A good experimental plan (such as D-optimal design) will however ensure that the variables are varied as independently as possible.

The operation points were run in the order 1, 7, 2, 8, 3, 4, 5, 6 for all catalyst configurations to make as large changes as possible in as many variables as possible. For some of the configurations several additional sequences were also run. To achieve steady state conditions all points were run for 15 minutes each. With very good reproducibility for all catalyst configurations, one of each of the transients 1 to 7, 2 to 8, 3 to 4, and 5 to 6 were selected for every catalyst, thereby reducing the used experimental data to two hours per catalyst configuration.

When starting simulations with the catalyst model the only known conditions were those of the inlet and outlet flow. This meant that initial properties such as concentrations and temperature inside the catalyst needed to be assumed which resulted in the first seconds of every simulation being unreliable. To avoid parameters being tuned against unreliable simulation results the first 120 s of every transient was removed from the calculation of the residual.

Several different optimization methods can be used to minimize the simulated residuals and the most common method is probably the gradient search method which was also the method used in this study. The method is very efficient for linear systems but can also be applied for non-linear systems such as catalyst models. For a non-linear system the residual function is first linearized for all parameters and then a step in

the parameter space is made in the direction of the steepest descent. This process is repeated until the change in residual is below a certain tolerance. For a thorough description of this method see for example [33]. The parameter tuning was not only complicated by the non-linearity of the system but also by the high correlation of the estimated parameters. The scope of this study did, however, not include a method for parameter sensitivity analysis or calculation of confidence intervals.

The gradient search method of choice in this work was the trust-region-reflective method [34]. This is the standard method for over determined non-linear least square problems in Matlab, the software used in this project. This method is implemented in the Matlab function lsqnonlin.

The heat production from the reactions taking place in the DOC was small compared to the convective heat transport due to gas flow and heat losses to the environment. This means that the kinetic parameters and the mass transport parameters will have only a small influence on the outlet temperature and thus the heat transfer parameters can be estimated separately.

The influence from the temperature on the reaction rates is however substantial which means that a good estimation of the heat transfer parameters is an important foundation for tuning the kinetic and mass transport parameters. The heat transfer parameters were therefore estimated before the other parameters and since temperature will not be affected by other parameter values they were not re-tuned later on. When the heat transfer parameters were calculated the only residual used was outlet temperature.

When parameter tuning of the kinetic and mass transport parameters was performed the simulated outlet concentrations of NO, NO<sub>2</sub>, HC and CO were compared to measurement data to form the model residuals. To avoid having the residuals from the higher concentration components dominate the parameter tuning, all residuals for a certain component were weighted by their average outlet concentration. This meant that the residuals of NO<sub>x</sub> were decreased in relation to the residuals of HC and CO.

To verify the significance of estimating effective diffusivity and including internal transport resistance in the models, parameter estimations were performed according to three different modes summarized in [table 3](#).

Table 3. Short description of the modes of Parameter Estimation

Nr	Modes of Parameter Estimation	Number of parameters	Discretization	
			Seg-ments	Lay-ers
1	Negligible internal mass transfer resistance	17	10	8*
2	Discretized washcoat and fixed effective diffusivity	17	10	8
3	Discretized washcoat and tuned effective diffusivity	19	10	8

\*Since concentration gradients in the washcoat were expected to be absent, two layers would have sufficed for this case, however eight layers were used for computational consistency

Mode 1 represents a case where the effective diffusivities were set to very high values (1000 times initial estimates) which, in effect, makes it a case with negligible internal transport resistance. Mode 2 and Mode 3 differ only by the fact that the latter has enabled estimation of the effective diffusivity whereas the former has not. For Mode 2 the effective diffusivities were fixed at the initially estimated values (see [equation A22](#) in appendix). Mode 3 uses one effective diffusivity scaling factor for small molecules and one for large molecules where all components except HC are considered small.

## RESULTS AND DISCUSSION

### Heat Transfer Parameter Tuning

The heat transfer parameters thermal mass ( $s_{\text{heat}}$ ), environmental temperature ( $T_{\infty}$ ), and lumped heat transfer coefficient ( $\alpha_{\text{tot}}$ ) were tuned before any additional parameter tuning was performed. The final values of the temperature parameters are shown in [table 4](#).

Table 4. Results of heat transfer parameter tuning

Parameter	Value
$s_{\text{heat}}$	4.7 kJ/K
$T_{\infty}$	112.2 °C
$\alpha_{\text{tot}}$	5.0 J/K,s

Note that these parameters are lumped to account for several different phenomena and therefore are difficult to interpret physically. The results for one of the catalyst configurations are shown in [figure 9](#).

The simulated temperature shows a good fit both during the fast transient changes in inlet temperature and the slower approach to steady states. The largest errors occur during high exhaust flow at high temperature (2700-3600 s) where the model under-predicts the heat loss and during low flow at low temperature (3600-4500 s) where the model over-predicts the heat loss. The maximum temperature deviation was 20 °C with the root mean square average being 3.6 °C. With only three parameters to tune, a perfect fit can however not be expected for all time points and thus the tuned temperature parameters were deemed good enough for continued parameter tuning of the kinetic and mass transport parameters considering the level of detail of the single channel model used. If the heat transfer parameters would not be included in the model the simulated outlet temperature would be close to the inlet temperature since the heats of reactions will have a minor effect on the temperature.

If only the measured temperatures in [figure 9](#) are studied, it is evident that the temperatures of all engine operating points were not stabilized even after 15 minutes (most apparently point 3 at 1800-2700 s). The temperature is however the only variable in [table 2](#) for which this was the case.

## Catalyst Parameter Tuning

The final results of the tuning of the kinetic parameters for the different parameter estimation modes are summarized in [table 6](#). Since catalyst configuration c (see [table 1](#)) consists of the catalyst in configuration a in series with another identical catalyst, the same activity scaling factor is assumed for both configuration a and c.

For Mode 3 an effective diffusivity scaling (see [equation A22](#)) for small components (NO, NO<sub>2</sub>, CO and O<sub>2</sub>) and large components (HC) were also tuned where the final tuning gave a value 7.71 times the initial estimate for the effective diffusivity for small components and a value 2.11 times the initial estimate for the effective diffusivity for large components. The correlation between the activity scaling factors and pre-exponential factors in the numerator of the rate expressions ( $A_{1-3}$ ) were linear. Equal changes in either the activity scaling factor or pre-exponential factor gave identical changes in the reaction rate. This was the case since the kinetic model only uses one type of reaction site.

The activity scaling factor was only intended to serve as a handle to tune differences in properties of the catalysts, such as metal dispersion, and should only be interpreted as a relative difference and not an absolute value for activity scaling. During the parameter tuning an upper limit of 1% for the activity scaling factors was therefore applied in order to facilitate the comparison between the three modes.

In general it can be expected that a high noble metal loading should correspond to a low dispersion and thereby also a lower activity scaling factor. It is therefore surprising that none of the modes have the highest activity scaling factor for the lowest loading, i.e. 0.30 wt% Pt loading ( $act_a$  and  $act_c$ ). Both Mode 1 and 3 have the highest activity scaling factor for configuration d where the washcoat is thinner than for the other configurations and has a high loading of 0.59 wt% Pt. Whereas, Mode 3 has the highest activity scaling factor for catalyst configuration b where the loading is also 0.59 wt% Pt. It should however be mentioned that the differences between the activity scaling factors are rather small.

The complexity of the kinetic model and the catalyst model complicates a thorough analysis of every single parameter value but some general remarks can be made. The original parameters over-predicted the conversion for all components and gave a very poor fit in general. The tuned parameters have therefore been changed in a direction where the reaction rates in general are slower. This is not always obvious when examining the parameter values since a large pre-exponential factor in the numerator ( $A_{1-3}$ ) may be compensated by a large pre-exponential factor in the denominator ( $A_{4-7}$ ) and differences in activation energies ( $E_{A,j}$ ) will make different pre-exponential factors significant at different temperatures. Mode 2 and 3 both show reduced pre-exponential factors in the numerator for all reactions which leads to reduced reaction rates. Mode 1 on the other hand has increased pre-exponential factors in the

numerator for both reaction 1 and 3 (CO and NO oxidation). This, together with the fact that Mode 1 has negligible internal mass transfer resistance, would lead to a significantly increased reaction rate compared to the start values if it was not for the simultaneous increase of  $A_7$  with about 3 orders of magnitude. A high value for the pre-exponential factor  $A_7$  will decrease all reaction rates since it is a part of the common denominator G (see [equation 5](#)) for all reaction rate expressions. The assumed physical interpretation of  $K_7 y_{NO}^{0.7}$ , where  $A_7$  is included, is the inhibiting effect of adsorbed NO on the surface. Since all NO is never consumed due to thermodynamic limitations, this factor will always influence the reaction rates of Mode 1 and generally cause them to be slower than for the start parameter values. This trend can also to a lesser extent be observed for Mode 3 but for Mode 2 the influence of the pre-exponential factor  $A_7$  is small.

If the other pre-exponential factors and activation energies used in the common denominator G are studied, it becomes clear that  $A_6$  and  $E_{A,6}$  are insignificant for the simulation results. The highest value of the factor  $1+K_6 y_{CO}^2 y_{HC}^2$  for all modes and simulated time points is 1.1 and more than 99.9% of the values are below 1.01. In the data used to formulate the original kinetic model proposed by Voltz et al. [6], the molar fractions of HC and CO were considerably higher than those measured in the current study. It is therefore possible that the inhibition by HC-CO interaction is no longer an issue for a modern engine exhaust and this inhibition term could be omitted from the kinetic model. However, the factor  $1+K_4 y_{CO}+K_5 y_{HC}$  has a mean of 5.47 and a maximum of 99.75 and is significant for all modes.

Under equal conditions the reaction rates of Mode 2 were significantly larger than the reaction rates of Mode 1 showing that the kinetic parameters in Mode 2 needed to compensate for internal transport resistance.

The scaling of the effective diffusivity performed in Mode 3 resulted in a reduction in the internal transport resistance for all species. If the parameter values are studied, it can be seen that for Mode 3 they are in most cases between the values for Mode 1 and Mode 2. This is of course not unexpected, since the effective diffusivities of Mode 3 have values between the effective diffusivities of Mode 1 and Mode 2.

If the trends in the pre-exponential factors were fairly clear the relations between activation energies were more complicated. The differences between the modes were relatively small and usually close to the initial value which could indicate that the activation energies are not as case specific as the pre-exponential factors. If the activation energy (or heat of adsorption)  $E_{A,7}$  is studied it should be noted that the sign is positive and opposite to the other activation energies in the denominator. This means that the inhibition by NO will increase with temperature and that this factor will result in a reduction of the reaction rate with temperature. In other words, it is the same kind of phenomena that transport resistance would cause and could explain the success of parameter estimation

with this kinetic model where internal transport has been neglected in the catalyst model (Mode 1). It is not physically realistic for an adsorption enthalpy to be endothermic, thus it is questionable whether the term  $K_7 y_{\text{NO}}^{0.7}$  truly accounts for NO inhibition. The reported values of  $E_{A,7}$  are positive both originally by Voltz et al. [6] and in other applications of the kinetic model [13]. It should, however, be mentioned that  $E_{A,7}$  also may indirectly account for  $\text{NO}_2$  inhibition that is not otherwise included in the kinetic model, since an increase in temperature could lead to higher  $\text{NO}_2$  concentration and thereby more  $\text{NO}_2$  inhibition.

### Model Fit

Two examples of the final results of the tuning of the kinetic and mass transport parameters for the different parameter estimation modes are shown in figures 10 and 11

Since the kinetic model did not account for  $\text{NO}_x$  reduction and since the difference between inlet and outlet  $\text{NO}_x$  in measurement data was small (<25 ppm), the modeling of NO and  $\text{NO}_2$  was considered well enough described by only NO concentration for the different parameter estimation modes

Figure 10 shows a good fit for all components for parameter estimation performed according to Mode 3 and a good fit for Mode 1 except for low HC conversion after the operating point change. The model where effective diffusivity was not tuned (Mode 2) shows a good fit except for NO before the operating point change.

Figure 11 shows that only the model where transport resistance was neglected (Mode 1) shows a good fit for NO. Mode 2 had a poor fit for the CO transient and appears to approach the wrong stationary values for both HC and CO. The transient behaviour of both HC and CO, before the change in operating point, was captured well by Mode 3 and more weakly by Mode 1. Both these modes approach the same stationary concentrations for HC (very good) and CO (good).

The above figures show only two of 16 transients used for parameter estimation (4 catalyst configurations and 4 operating point changes for every configuration). The transients were selected to give a wide temperature and concentration window. Specifically, the results of figure 11 were chosen since the conversions of both HC and CO were below 100 % for operating point 2, which along with operating point 1, were the only points with this feature. In addition, the high temperature at the start of the experiment provided an interesting transient change in both CO and HC conversion for the first 900 s. The transient in figure 10 was chosen since the temperatures were high enough for the NO oxidation to take place, but still low enough to only reach 85% of thermodynamic equilibrium. To give an overview of the simulation results the residual sum of squares for every mode and component is shown in table 5. Note that the residuals in this table have been weighted with

the inverse of the average concentrations for the entire data set according to the method previously described in *Parameter Estimation Method*.

Table 5. Residual sum of squares ( $\times 10^5$ ) of every component together with the summation of residual sum of squares (rightmost column) for the different modes.

	NO	HC	CO	$\text{NO}_2$	Sum
Mode 1	0.67	3.10	4.46	0.83	9.05
Mode 2	2.09	2.44	6.89	2.64	14.1
Mode 3	0.77	2.41	3.49	0.97	7.65

### Analysis of Kinetic Model Structure

The initial kinetic parameters shown in table 6 were collected from lab scale data, where the transport resistance was assumed to be negligible. Mode 2 has by far the highest residual sum of squares and it may therefore be speculated that the difficulties encountered when tuning a model where the transport resistance is not neglected, could indicate that the original parameters were in fact influenced by transport resistance. The structure of the kinetic model itself may also make it less suitable for a catalyst model where the internal transport resistance is clearly separated from the kinetics. The basis for this conclusion is that the positive value of the activation energy (or heat of adsorption) for NO inhibition ( $E_{A,7}$ ), discussed previously, which reduces reaction rates with increased temperature similar to the effects of internal transport resistance. This could then explain why the results of Mode 1, where the transport resistance was neglected, showed a better fit for  $\text{NO}_x$  which can be seen in both table 5 and figures 10 and 11. In a model that clearly separates mass transport and kinetics, it is in other words not only important to have original parameters uninfluenced by transport resistance, but also that the kinetic model itself should not have the possibility to mimic internal transport effects.

The common denominator G of the reaction rate expressions, shown in equation 5, can be split up into its three factors;  $G_1 = (1 + K_4 y_{\text{CO}} + K_5 y_{\text{C}_3\text{H}_6})^2$ ,  $G_2 = 1 + K_6 y_{\text{CO}}^2 y_{\text{C}_3\text{H}_6}^2$ , and  $G_3 = 1 + K_7 y_{\text{NO}}^{0.7}$ . As previously stated,  $G_2$  according to the values of  $A_6$  and  $E_{A,6}$  was insignificant for the simulation results which means that it will be sufficient to only consider  $G_1$  and  $G_3$  to illustrate the influence of G on the reaction rates. In figure 12,  $G_1$  and  $G_3$  are shown for the two experiments previously analyzed in figures 10 and 11 at one position in the catalyst washcoat (segment 10 and layer 1). Since the nominator will be different for the three modes a comparison of the G-factors will be more informative if the total G is also shown in relation to some reference value for the mode in question. Figures 12 (e) and (f) therefore show G relative to the maximum of G for the selected transient and mode.

Table 6. Results of kinetic parameter tuning.

	A <sub>1</sub> [mol,K/m <sup>2</sup> ,s]	A <sub>2</sub> [mol,K/m <sup>2</sup> ,s]	A <sub>3</sub> [mol,K/m <sup>2</sup> ,s]	A <sub>4</sub> [-]	A <sub>5</sub> [-]	A <sub>6</sub> [-]	A <sub>7</sub> [-]	E <sub>A,1</sub> [J/mol]
<b>Initial [13]</b>	100×10 <sup>15</sup>	400×10 <sup>18</sup>	45.0×10 <sup>13</sup>	65.5	2.08×10 <sup>3</sup>	3.98	4.79×10 <sup>5</sup>	8.00×10 <sup>4</sup>
<b>Mode 1</b>	404×10 <sup>15</sup>	118×10 <sup>18</sup>	119×10 <sup>13</sup>	22.1	50.1×10 <sup>3</sup>	0.479	4888×10 <sup>5</sup>	7.66×10 <sup>4</sup>
<b>Mode 2</b>	3.90×10 <sup>15</sup>	0.516×10 <sup>18</sup>	0.183×10 <sup>13</sup>	233	24.4×10 <sup>3</sup>	6.58	2.11×10 <sup>5</sup>	7.95×10 <sup>4</sup>
<b>Mode 3</b>	48.9×10 <sup>15</sup>	12.5×10 <sup>18</sup>	27.1×10 <sup>13</sup>	95.8	82.5×10 <sup>3</sup>	1.93	471×10 <sup>5</sup>	7.67×10 <sup>4</sup>

	E <sub>A,2</sub> [J/mol]	E <sub>A,3</sub> [J/mol]	E <sub>A,4</sub> [J/mol]	E <sub>A,5</sub> [J/mol]	E <sub>A,6</sub> [J/mol]	E <sub>A,7</sub> [J/mol]	act <sub>a</sub> . act <sub>c</sub> [%]	act <sub>b</sub> [%]	act <sub>d</sub> [%]
<b>Initial [13]</b>	10.0×10 <sup>4</sup>	7.00×10 <sup>4</sup>	-7.99×10 <sup>3</sup>	-3.00×10 <sup>3</sup>	-9.65×10 <sup>4</sup>	3.10×10 <sup>4</sup>	1.00	1.00	1.00
<b>Mode 1</b>	9.86×10 <sup>4</sup>	7.00×10 <sup>4</sup>	-10.6×10 <sup>3</sup>	-2.01×10 <sup>3</sup>	-9.77×10 <sup>4</sup>	2.94×10 <sup>4</sup>	0.792	0.751	1.00
<b>Mode 2</b>	10.0×10 <sup>4</sup>	7.23×10 <sup>4</sup>	-8.32×10 <sup>3</sup>	-2.55×10 <sup>3</sup>	-9.64×10 <sup>4</sup>	3.11×10 <sup>4</sup>	0.707	1.00	0.734
<b>Mode 3</b>	9.80×10 <sup>4</sup>	7.46×10 <sup>4</sup>	-8.06×10 <sup>3</sup>	-1.64×10 <sup>3</sup>	-9.69×10 <sup>4</sup>	3.05×10 <sup>4</sup>	0.766	0.701	1.00

\* act<sub>a</sub> is activity scaling factor for catalyst configuration a (0.30 wt% Pt), act<sub>b</sub> is activity scaling factor for catalyst configuration b (0.59 wt% Pt), and act<sub>d</sub> is activity scaling factor for catalyst configuration d (0.59 wt% Pt with thin washcoat).

When figure 12 is studied the most apparent difference between the modes appear to be the much higher values for  $G_3$  for mode 1 which is shown in panels c and d. Since  $E_{A,7}$  has similar values for all three modes the temperature dependence of  $G_3$  will also be similar, which can be seen in panels c and d. The large difference in  $A_7$  will however amplify the behavior of mode 1 more than the others. Figure 7 (a) and (b) show that mode 3 has the largest  $G_1$  factor, indicating a somewhat more pronounced inhibition of CO and HC. The most informative part of figure 12 may be panels e and f since the relative values of  $G$  simplifies the comparison of the modes and their  $G$  expressions. In panel e modes 2 and 3 are close to constant before and after the change in operating point caused by an increase in  $G_3$  and a decrease in  $G_1$  as the operating point is changed. For mode 1 on the other hand,  $G$  decreases by about 30 % as a result of the dominating influence of the strong temperature dependence of  $G_3$ . In panel f the  $G$  of both mode 1 and 3 increase after the change in operating point but the relative change for mode 1 is noticeably larger than that for mode 3. The relative increase in  $G$  for mode 1 is about 200% but for mode 3 it is only about 75%. This means that  $G$  will have a negative influence on reaction rates for both modes even though the temperature is increasing, however the trend is much stronger for mode 1. The previous speculation that a high value of  $A_7$  for mode 1 contributes to a decrease in reaction rates with increasing temperature has in other words been confirmed from the analysis of panels c, d, e, and f of figure 12.

### Analysis of Transport Resistance

The results with Mode 3 displayed an overall better fit than for Mode 2 which is also evident when the total residual sum of squares are compared (table 5). This would indicate that the tuning of transport resistance parameters is very important for the overall behaviour of the model. For Mode 3 the effective diffusivities for all molecules were increased compared to their initial estimates which means that the behavior of the model has moved closer to a model with negligible transport

resistance like Mode 1. This could mean that the washcoat properties, such as the tortuosity and porosity or even the average washcoat thickness were not known with sufficient accuracy. In addition, the precision of the model used to estimate the effective diffusivities (eq. A22) can be questioned. It is apparent from the analysis that there is correlation between one inhibition factor ( $G_3$ ) and internal transport resistance. There is a risk, that even with Mode 3, their effects are not fully discriminated which means the effective diffusivities were increased to compensate for inhibition factor  $G_3$ . As a result the values of effective diffusivity arrived at from Mode 3 may not be generally applicable, but instead specific to this kinetic model.

The importance of internal transport resistance is commonly diagnosed by the so called Weisz modulus which is defined by equation 7 and calculated here according equation to 8.

$$C_{WP} = \frac{\text{observed reaction rate}}{\text{maximum diffusion rate}} \quad (7)$$

$$C_{WPI,k} = \frac{W^2 \sum_n \frac{\Gamma_{j,k,n} A_{m,k,n}}{V_{k,n}}}{D_{eff,i,k} C_{surf,i,k}} \quad (8)$$

$C_{WPI,k}$  is the Weisz modulus for monolith segment  $k$  and species  $i$ .  $C_{surf,i,k}$  is the surface concentration of species  $i$  calculated from the gas bulk concentration and the concentration in the first layer. A value of  $C_{WP}$  much smaller than one indicates negligible internal transport resistance and a value much larger than one indicates severe internal transport resistance. In figure 4 the Weisz modulus is plotted for the NO oxidation reaction at the monolith inlet and a comparison between the results of Mode 2 and 3 is made. Experimental points, where the outlet conversion was greater than 90% of the thermodynamic equilibrium, were excluded from figure 4. The reason behind this exclusion of a large

amount of the data points is that only conditions where reaction kinetics and/or internal transport resistances limited the process were considered of value for estimating the kinetic and mass transport parameters. In [figure 5](#) the Weisz modulus is plotted for the HC oxidation reaction at the monolith inlet and for this case experimental points where the outlet conversion was greater than 90% for HC were excluded. The total number of points is however still large in both [figure 4](#) and [5](#) since data points from all simulations were used in the selections.

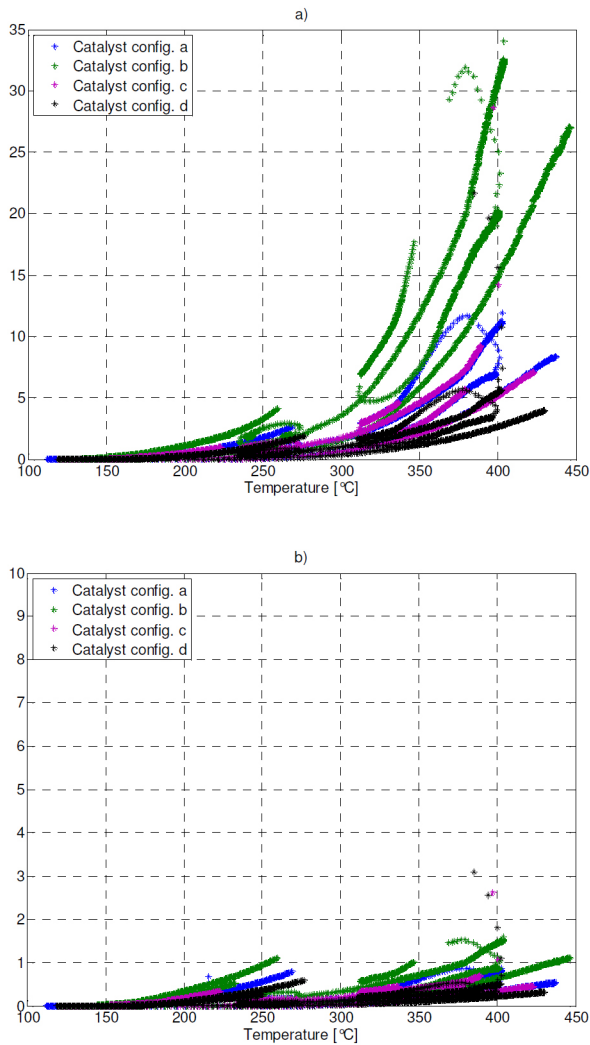


Figure 4. Weisz modulus for NO oxidation at monolith inlet for configurations a-d. a) Weisz modulus for Mode 2 and b) Weisz modulus for Mode 3

[Figure 4](#) shows that there is a significant difference between the internal transport resistances for Mode 2 and 3. At the lowest temperatures the internal transport resistances is close to negligible, whereas at higher temperatures this is not the case. As expected the transport limitations were less severe for Mode 3, since the effective diffusivities for NO were about

seven times greater than the values in Mode 2. Still for Mode 3, internal transport resistance was prevalent over a range of higher temperatures. [Figure 4](#) also shows that the Weisz modulus is highest for catalyst configuration b which is a result of this configuration having the highest platinum loading (0.59 wt%Pt) in combination with a higher washcoat thickness than catalyst configuration d with the same platinum loading. Comparing catalyst configurations a and d also shows that reducing the washcoat thickness but maintaining the total Pt mass reduced the transport limitations as expected.

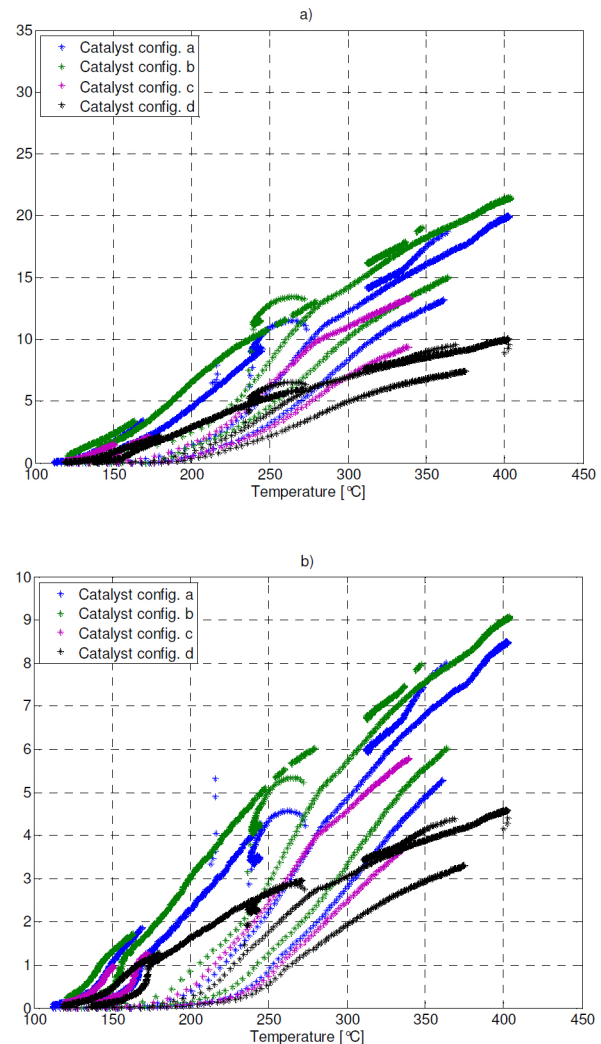


Figure 5. Weisz modulus for HC oxidation in first segment for catalyst configurations a-d. Panel a) shows Weisz modulus for Mode 2 and panel b) shows Weisz modulus for Mode 3

If the Weisz modulus of HC oxidation is studied it is evident that there is a distinct difference between Mode 2 and Mode 3 ([figure 5](#)). The internal transport limitations for Mode 3 are also more evident for HC oxidation than for the NO oxidation which should be expected since both the original diffusivity and the diffusivity scaling is smaller for HC than for the other components. The trends for the Weisz modulus for CO oxidation (not shown) were similar to that for NO oxidation.

The analysis of the Weisz modulus is strictly based on simulation data and to get a confirmation of mass transfer limitations in the measurement data additional analysis is necessary. In [figure 6](#) the temperature dependence of the conversion of NO is shown for three different transients and two catalyst configurations. The NO conversion is calculated relative to the thermodynamic limitation, which means that a 100% conversion

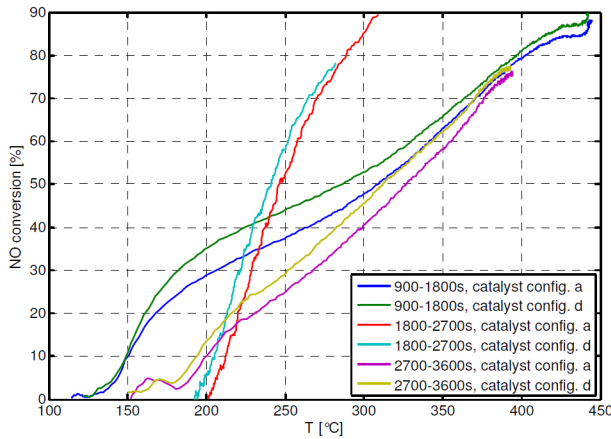


Figure 6. Comparison of NO conversion between catalyst configuration a and d at three different transients in temperature occurring between 900 s and 2700 s of the simulation shown in [figure 9](#).

As another example of internal transport resistance in the washcoat, the concentration gradients for HC are shown for the different modes in [figure 7](#). The Weisz moduli for HC oxidation at the depicted time point were  $1.0 \times 10^{-3}$ , 1.4 and 0.4 for Mode 1-3 respectively which illustrates what concentration gradients can be expected at different values of the Weisz modulus.

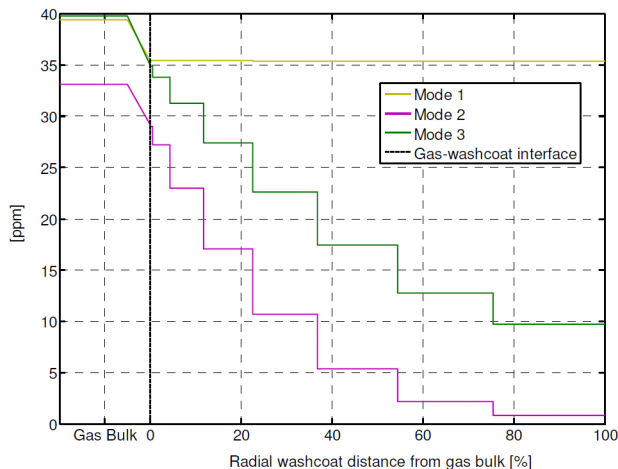


Figure 7. Radial concentration gradients of HC for the different modes at the monolith outlet. The time is 600 s into the experiment shown in [figure 10](#) where engine operating point 2 is run with catalyst configuration b.

In [figure 7](#) the concentrations in the gas bulk are shown for the different modes at a certain time point. The concentration gradient in the gas film is depicted as a line between the gas bulk concentration and the washcoat surface concentration. The length of both this line and the line describing the gas bulk concentration is arbitrary. If the gas-washcoat interface in [figure 7](#) is studied it is possible to distinguish that the concentration at the washcoat surface is not the same as in the first washcoat layer. This is a result of the lumping of the film resistance and the internal resistance in the first layer according to [equation A3](#).

Since Mode 1 has film resistance as the only mass transport resistance, the concentration profile is, as expected, flat with exception of the gradient in the film. The concentration gradient for Mode 2 is somewhat steeper than for Mode 3 which is a result of the increased effective diffusivity estimated in Mode 3. To illustrate the gradients in [figure 7](#) in a wider perspective the axial and radial concentration gradients for Mode 3 are shown in [figure 8](#).

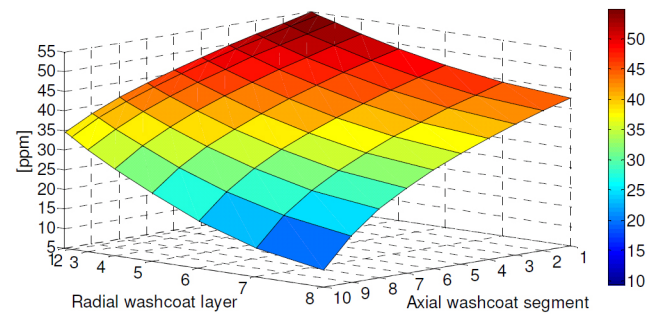


Figure 8. Radial and axial concentration gradients of HC for Mode 3 at 600 s into the experiment shown in [figure 10](#) (catalyst configuration b, operating point 2)

[Figure 8](#) shows significant concentration gradients both axially and radially in the washcoat. Both the axial and radial concentration gradients increase closer to the catalyst outlet which is a result of higher temperature and lower concentrations of inhibiting species at the catalyst outlet at this time point. The higher temperature close to the outlet is a result of heat stored from the previous engine operating point that had a higher exhaust temperature (see temperature at time 0 s in [figure 10](#)).

Both the concentration gradients in [figure 7](#) and [8](#), and the Weisz moduli analysis in [figures 4](#) and [5](#) show that internal transport resistance will likely influence the conversion in a full scale DOC at certain engine operating points. The fact that the model (Mode 1) with negligible internal transport resistance also shows a good general fit can mainly be attributed to the fact that the kinetics includes parameters enabling it to mimic transport resistance, which was shown in [figure 12](#). This highlights that it is not only important to determine the original kinetic parameters under intrinsic conditions but that it is equally important that the kinetic model itself has an intrinsic structure. The Mode 1 configuration will likely not be as successful if applied to a more complex system of mass

transport and reaction, such as a dual layer catalyst or a DOC with washcoat thickness beyond the range studied here, where the temperature dependence of G3 may not be enough to successfully mimic the transport resistance. A kinetic model

free from mass transfer effects would have probably resulted in a worse fit for Mode 1 and at the same time making an improved fit for Mode 2 and Mode 3 possible.

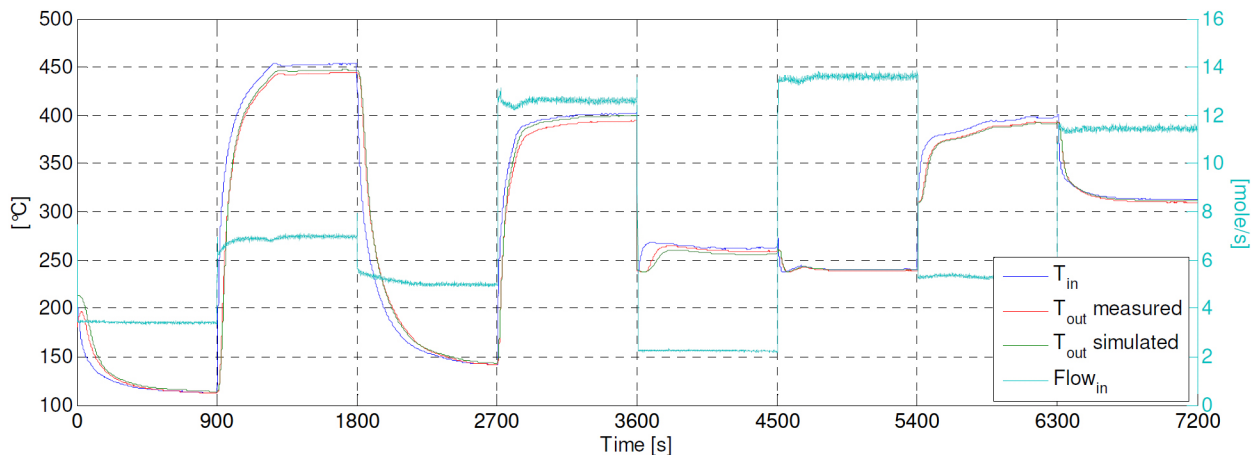


Figure 9. Measured inlet and outlet temperature transients for configuration d, steps between operation points 1 to 7, 2 to 8, 3 to 4 and 5 to 6 together with simulated results with estimated temperature parameters.

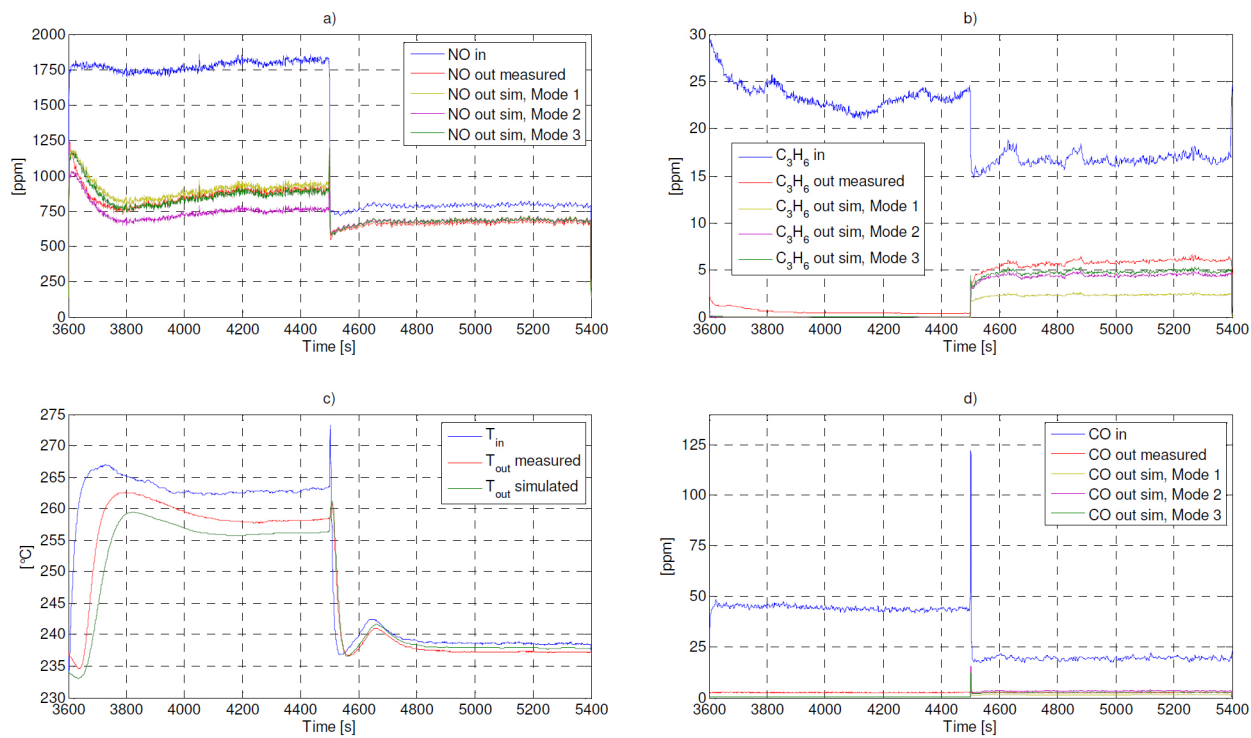


Figure 10. Measured and simulated outlet concentrations of NO (a),  $C_3H_6$  (b), CO (d) and temperature (c) for a change in operating point from 3 to 4 for catalyst configuration d. The three different modes of parameter estimation are described in [table 3](#).

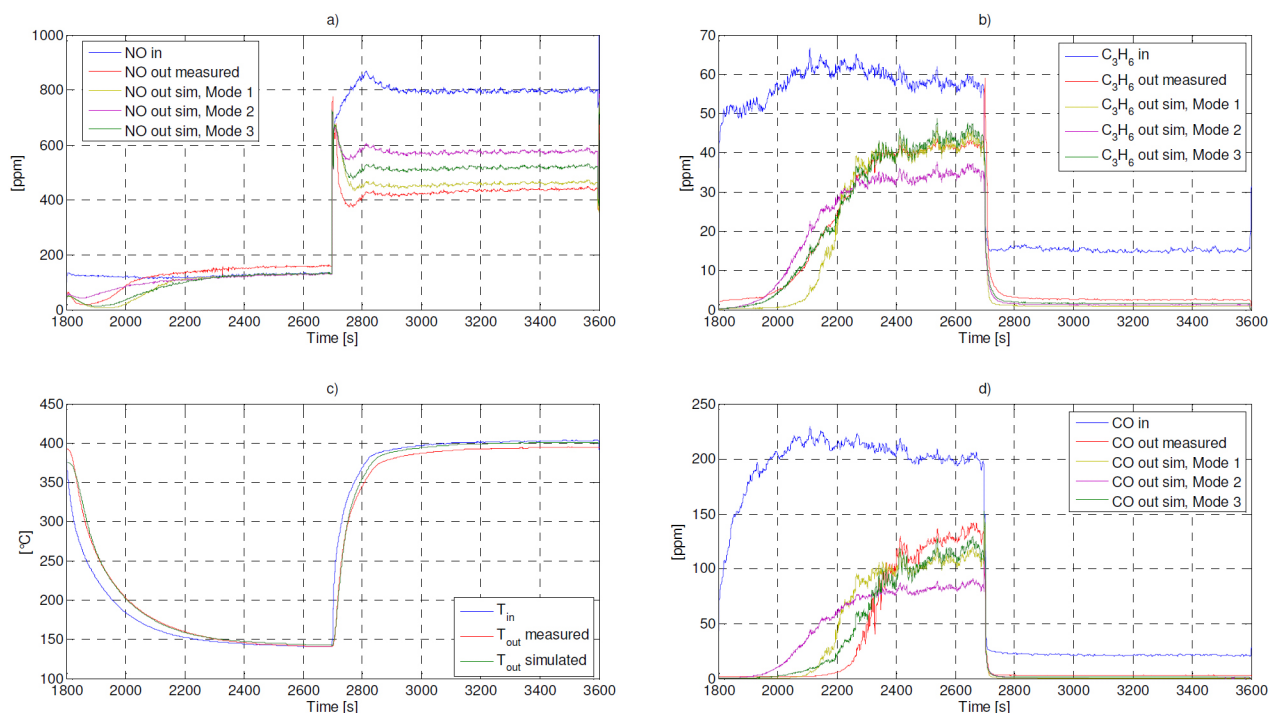


Figure 11. Measured and simulated outlet concentrations of NO (a), C<sub>3</sub>H<sub>6</sub> (b), CO (d) and temperature (c) for a change in operating point from 2 to 8 for catalyst configuration b. The three different modes of parameter estimation are described in table 3.

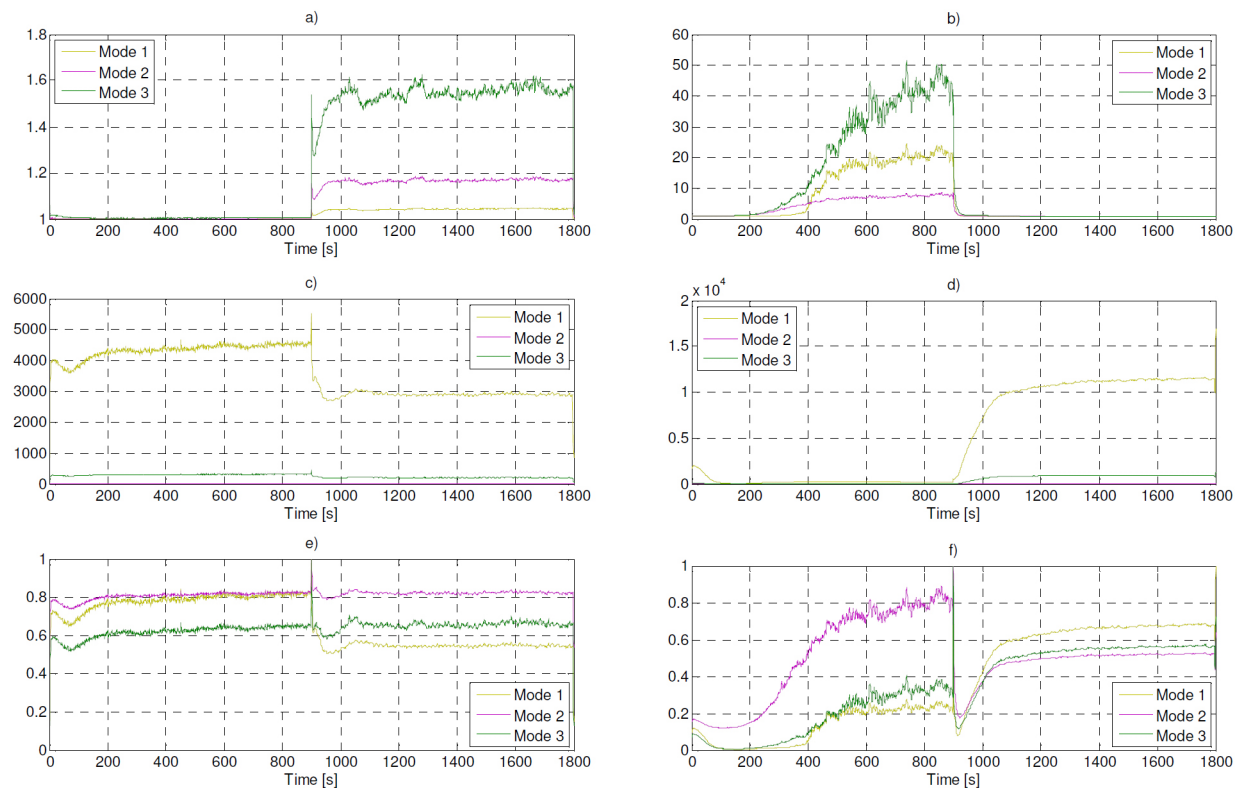


Figure 12. Factors of the common denominator G of the reaction rate expressions in segment 10 and layer 1. Figures to the left correspond to the experiment in figure 10 and figures to the right correspond to the experiment in figure 11. a), b) G factor one,  $(1+K_4y_{CO}+K_5y_{C_3H_6})^2$ . c), d) G factor three,  $1+K_7y_{NO}^{0.7}$ . e), f) G relative to maximum G.

## CONCLUSIONS

The wide range of catalyst configurations used has together with the data that is both stationary and transient made it possible to tune, not only kinetic parameters, but also parameters influencing transport resistance in the washcoat. By tuning parameters to data from engine measurements on different catalysts with different kinetic and mass transport properties the influence from transport phenomena on kinetic parameters was reduced. Some conclusions about the method of parameter estimation could be made by evaluating three different catalyst model formulations:

- In a catalyst model with internal transport resistance the best fit could be achieved if some parameters affecting the internal mass transport (in this study effective diffusivity) were tuned in addition to the kinetic parameters. This indicates that internal transport limitations can be of importance for a DOC in a heavy-duty vehicle aftertreatment system, particularly for HC oxidation but also to a certain extent for NO and CO oxidation.
- The simultaneous tuning of kinetic parameters and mass transport parameters depend on an experimental design for this purpose, which has been shown in this study. The conditions for the tuning of mass transport parameters are specifically improved by a wide range of available catalyst configurations with varying internal transport resistances.
- With a model with negligible internal transport resistance it is still possible to obtain a good fit since kinetic parameters could compensate for transport limitations. This highlights the inherent difficulties using kinetic models with high parameter correlation and also shows the importance of using a kinetic model with a structure capable of describing exclusively intrinsic kinetics.
- Activity scaling factors were found not to be correlated with the noble metal loading. Instead they likely accounted for other differences in the properties of catalyst samples that the simple kinetic model used here did not include.
- Due to the correlation between the inhibition factor ( $G_3$ ) and the internal transport resistance it is difficult to with certainty conclude that the effective diffusivities determined are separated from the influence of kinetics. The estimated kinetic parameters and effective diffusivities may therefore still be specific for the catalyst configurations used in the experiments.

## REFERENCES

1. Metkar, P.S., Salazar N., Muncrief R., Balakotaiah V., et al., *Selective catalytic reduction of NO with NH<sub>3</sub> on iron zeolite monolithic catalysts: Steady-state and transient kinetics*. Applied Catalysis B: Environmental, 2011. 104(1-2): p. 110-126.
2. Sukumar, B., Dai, J., Johansson, A., Markatou, P. et al., "Modeling of Dual Layer Ammonia Slip Catalysts (ASC)," SAE Technical Paper 2012-01-1294, 2012, doi:10.4271/2012-01-1294.
3. Hayes, R.E. and Kolaczkowski S.T., *Mass and heat transfer effects in catalytic monolith reactors*. Chemical Engineering Science, 1994. 49(21): p. 3587-3599.
4. Holmgren, A. and Andersson B., *Mass transfer in monolith catalysts-CO oxidation experiments and simulations*. Chemical Engineering Science, 1998. 53(13): p. 2285-2298.
5. Nova, I., Bounechada D., Maestri R., Tronconi E., et al., *Influence of the Substrate Properties on the Performances of NH<sub>3</sub>-SCR Monolithic Catalysts for the Aftertreatment of Diesel Exhaust: An Experimental and Modeling Study*. Industrial & Engineering Chemistry Research, 2010. 50(1): p. 299-309.
6. Voltz, S.E., Morgan C.R., Liederma D., and Jacob S.M., *Kinetic Study of Carbon Monoxide and Propylene Oxidation on Platinum Catalysts*. Product R&D, 1973. 12(4): p. 294-301.
7. Ansell, G.P., Bennett P.S., Cox J.P., Frost J.C., et al., *The development of a model capable of predicting diesel lean NOx catalyst performance under transient conditions*. Applied Catalysis B: Environmental, 1996. 10(1-3): p. 183-201.
8. Lafossas, F., Matsuda Y., Mohammadi A., Morishima A., et al., *Calibration and Validation of a Diesel Oxidation Catalyst Model: from Synthetic Gas Testing to Driving Cycle Applications*. 2011.
9. Watling, T., Ahmadinejad, M., Tuțuianu, M., Johansson, Å. et al., "Development and Validation of a Pt-Pd Diesel Oxidation Catalyst Model," *SAE Int. J. Engines* 5(3):1420-1442, 2012, doi:10.4271/2012-01-1286.
10. Crocoll, M., Kureti S., and Weisweiler W., *Mean field modeling of NO oxidation over Pt/Al<sub>2</sub>O<sub>3</sub> catalyst under oxygen-rich conditions*. Journal of Catalysis, 2005. 229(2): p. 480-489.
11. Olsson, L., Fridell E., Skoglundh M., and Andersson B., *Mean field modelling of NOx storage on Pt/BaO/Al<sub>2</sub>O<sub>3</sub>*. Catalysis Today, 2002. 73(3-4): p. 263-270.
12. Salomons, S., Votsmeier M., Hayes R.E., Drochner A., et al., *CO and H<sub>2</sub> oxidation on a platinum monolith diesel oxidation catalyst*. Catalysis Today, 2006. 117(4): p. 491-497.
13. Wang, T.J., Baek S.W., and Lee J.H., *Kinetic parameter estimation of a diesel oxidation catalyst under actual vehicle operating conditions*. Industrial & Engineering Chemistry Research, 2008. 47(8): p. 2528-2537.
14. Froment, G.F., De Wilde J., and Bischoff K.B., *Chemical reactor analysis and design*. Vol. 3rd ed. 2011, Hoboken, N.J: Wiley.
15. Kočí, P., Novák V., Štěpánek F., Marek M., et al., *Multi-scale modelling of reaction and transport in porous catalysts*. Chemical Engineering Science, 2010. 65(1): p. 412-419.
16. Novák, V., Kočí P., Marek M., Štěpánek F., et al., *Multi-scale modelling and measurements of diffusion through porous catalytic coatings: An application to exhaust gas oxidation*. Catalysis Today, 2012. 188(1): p. 62-69.
17. Kolaczkowski, S.T., *Measurement of effective diffusivity in catalyst-coated monoliths*. Catalysis Today, 2003. 83(1-4): p. 85-95.
18. Zhang, F., Hayes R.E., and Kolaczkowski S.T., *A New Technique to Measure the Effective Diffusivity in a Catalytic Monolith Washcoat*. Chemical Engineering Research and Design, 2004. 82(4): p. 481-489.
19. Ericson, C., Westerberg, B., and Odenbrand, I., "A State-Space Simplified SCR Catalyst Model for Real Time Applications," SAE Technical Paper 2008-01-0616, 2008, doi:10.4271/2008-01-0616.
20. Mladenov, N., Koop J., Tischer S., and Deutschmann O., *Modeling of transport and chemistry in channel flows of automotive catalytic converters*. Chemical Engineering Science, 2010. 65(2): p. 812-826.
21. Oh, S.H. and Cavendish J.C., *Transients of monolithic catalytic converters. Response to step changes in feedstream temperature as related to controlling automobile emissions*. Industrial & Engineering Chemistry Product Research and Development, 1982. 21(1): p. 29-37.
22. Stamatelos, A.M., Koltsakis G.C., Kandyas I.P., and Pontikakis G.N., *Computer aided engineering in diesel exhaust aftertreatment systems design*. Proceedings of the Institution of Mechanical Engineers, Part D (Journal of Automobile Engineering), 1999. 213(Copyright 2000, IEE): p. 545-60.
23. Pandya, A., Mmbaga J., Hayes R.E., Hauptmann W., et al., *Global kinetic model and parameter optimization for a diesel oxidation catalyst*. Topics in Catalysis, 2009. 52(13-20): p. 1929-1933.
24. Kandyas, I.P. and Koltsakis G.C., *NO<sub>2</sub>-Assisted Regeneration of Diesel Particulate Filters: A Modeling Study*. Industrial & Engineering Chemistry Research, 2002. 41(9): p. 2115-2123.
25. Guojiang, W. and Song T., *CFD simulation of the effect of upstream flow distribution on the light-off performance of a catalytic converter*. Energy Conversion and Management, 2005. 46(13-14): p. 2010-2031.

26. Tsinoglou, D.N. and Koltsakis G.C., *Effect of perturbations in the exhaust gas composition on three-way catalyst light off*. Chemical Engineering Science, 2003. 58(1): p. 179-192.
27. Koltsakis, G.C. and Stamatelos A.M., *Modeling dynamic phenomena in 3-way catalytic converters*. Chemical Engineering Science, 1999. 54(20): p. 4567-4578.
28. Dubien, C., Schweich D., Mabilon G., Martin B., et al., *Three-way catalytic converter modelling: fast and slow-oxidizing hydrocarbons, inhibiting species, and steam-reforming reaction*. Chemical Engineering Science, 1998. 53(3): p. 471-481.
29. Koltsakis, G.C., Konstantinidis P.A., and Stamatelos A.M., *Development and application range of mathematical models for 3-way catalytic converters*. Applied Catalysis B: Environmental, 1997. 12(2-3): p. 161-191.
30. Chen, D., Bissett, E., Oh, S., and Van Ostrom, D., "A Three-Dimensional Model for the Analysis of Transient Thermal and Conversion Characteristics of Monolithic Catalytic Converters," SAE Technical Paper 880282, 1988, doi:10.4271/880282.
31. Sjoblom, J. and Creaser D., *Latent variable projections of sensitivity data for experimental screening and kinetic modeling*. Computers & Chemical Engineering, 2008. 32(12): p. 3121-3129.
32. Hauff, K., Tuttlies U., Eigenberger G., and Nieken U., *A global description of DOC kinetics for catalysts with different platinum loadings and aging status*. Applied Catalysis B: Environmental, 2010. 100(1-2): p. 10-18.
33. Montgomery, D.C., *Design and Analysis of Experiments (7th Edition)*. 2009, John Wiley & Sons. p. 417-439.
34. Coleman, T.F. and Li Y.Y., *An interior trust region approach for nonlinear minimization subject to bounds*. Siam Journal on Optimization, 1996. 6(2): p. 418-445.
35. Tronconi, E. and Forzatti P., *Adequacy of Lumped Parameter Models for SCR Reactors with Monolith Structure*. Aiche Journal, 1992. 38(2): p. 201-210.
36. Murzin, D. and Salmi T., *Mass transfer and catalytic reactions, in Catalytic Kinetics*. 2005, Elsevier Science: Amsterdam. p. 341-418.
37. Box, G.E.P., Hunter W.G., MacGregor J.F., and Erjavec J., *Some Problems Associated with the Analysis of Multiresponse Data*. Technometrics, 1973. 15(1): p. 33-51.

$C_{WP,i,k}$	weisz modulus for segment k and species i [-]	
$d$	open channel width [m]	
$D_{eff,i,k}$	effective diffusivity for species i in channel segment k [m <sup>2</sup> /s]	
$D_{i,k}$	diffusivity for species i in channel segment k [m <sup>2</sup> /s]	
$DK_{i,k}$	knudsen diffusivity for species i in channel segment k [m <sup>2</sup> /s]	
$d_p$	mean pore diameter [m]	11.05×10 <sup>-9</sup>
$D_{ref,i}$	diffusivity for species i at reference temperature [m <sup>2</sup> /s]	
$E_{Aj}$	activation energy for reaction rate coefficient j [J/mol]	
$f_D$	porosity and tortuosity factor [-]	0.2125
$f_{D,scale,i}$	effective diffusivity scaling for species i	
$F_{tot}$	total flow [mol/s]	
$h_k$	heat transfer coefficient in channel segment k [W/m <sup>2</sup> ,K]	
$k_{c,i,k}$	mass transfer coefficient for species i in channel segment k [m/s]	
$k_j$	reaction rate coefficient j [mol,K/m <sup>2</sup> s]	
$K_j$	denominator reaction rate coefficient j [-]	
$k_{j,ref}$	reaction rate coefficient at reference temperature [mol,K/m <sup>2</sup> s]	
$K_p$	equilibrium constant for NO-oxidation	
$M_i$	molecular weight of species i [kg/mol]	
$m_{s,k,n}$	mass of solid material in channel segment k and layer n [kg]	
$Nu$	asymptotic Nusselt number used for monoliths [-]	2.5
$p$	estimated parameter	
$q_k$	solid heat flux from segment to segment k from up streams segment [J/m <sup>2</sup> ,s]	4.7×10 <sup>3</sup>
$R$	ideal gas constant	8.3144
$r_{j,k,n}$	reaction rate for reaction j in channel segment k and layer n [mole/m <sup>2</sup> , Pt, s]	
$Sh$	asymptotic Sherwood number used for monoliths [-]	2.5
$S_{heat}$	heat sink originating from solid material not included in the catalyst (e.g. catalyst canning and insulation) [J/K]	
$T_{\infty}$	environmental temperature (estimated) [K]	385.35
$T_{g,k}$	gas temperature in channel segment k [K]	
$T_{ref}$	reference temperature [K]	450
$T_{s,k}$	solid temperature in channel segment k [K]	
$W$	washcoat thickness [m]	
$w$	weight factor for parameter estimation	

## ACKNOWLEDGEMENT

The computations were performed on resources provided by the Swedish National Infrastructure for Computing (SNIC) at C3SE. Financial support from Swedish Energy Agency is gratefully acknowledged.

## NOMENCLATURE

Symbol	Description	Constant value (if available)
$A_j$	pre-exponential factor for reaction rate coefficient j [mol,K/m <sup>2</sup> s]	
$A_k$	mass and heat transfer area between layers [m <sup>3</sup> ]	
$A_{m,k,n}$	catalyst active surface area in channel segment k and wall layer n [m <sup>2</sup> ]	
$c_{i,k,n}$	concentration of species i in channel segment k and layer n [mol/m <sup>3</sup> ]	
$c_{p,g}$	gas heat capacity [J/mol,K]	31.6
$c_{p,s}$	solid heat capacity (mass weighted average of washcoat and substrate heat capacity) [J/kg,K]	
$c_{surf,i,k}$	surface concentration of species i in segment k [mol/m <sup>3</sup> ]	

$V_{k,n}$	volume of channel segment k and layer n [m <sup>3</sup> ]	
$y_{i,k,n}$	mole fraction of species i in channel segment k and layer n [mol/m <sup>3</sup> ]	
$\alpha_{tot}$	lumped parameter for heat loss to the environment [J/s,K]	5.0
$\Gamma_{i,k,n}$	lumped mass transfer coefficient for gas species i in segment k and layer n [m <sup>3</sup> /s]	
$\Delta H_j$	heat of reaction for reaction j [J/mol]	
$\Delta X_n$	thickness of layer n [m]	
$\Delta z_k$	length of channel segment k [m]	
$\epsilon$	washcoat porosity [-]	0.85
$\lambda_g$	gas thermal conductivity at reference temperature [W/m,K]	0.045
$\lambda_s$	solid heat conductivity [W/m,K]	0.4187
$\nu_{ij}$	stoichiometric coefficient for species i	
$\rho_{sub}$	substrate density [kg/m <sup>3</sup> ]	420
$\rho_{wsc}$	washcoat density [kg/m <sup>3</sup> ]	650

## SUBSCRIPTS AND SUPERSCRIPTS

Symbol	Description
$i$	species
$j$	reaction number
$k$	segment number (axial discretization)
$n$	layer number (radial discretization)
$o$	original value of estimated parameter
$Ea$	weight factor or estimated parameter for activation energy
$a$	weight factor or estimated parameter for pre-exponential factor
$D_{scale}$	weight factor or estimated parameter for effective diffusivity scaling
$T_\infty$	weight factor or estimated parameter for effective environmental temperature
$\alpha_{tot}$	weight factor or estimated parameter for lumped heat transfer parameter
$sheat$	weight factor or estimated parameter for lumped Heat sink parameter (sheat)

## APPENDIX

### REACTOR MODEL

#### Mass and Heat Balance

Quasi-steady state was considered to prevail for gas phase species (eq. A1-A2) and gas temperature (eq. A6) since the characteristic time constants are far shorter for these processes compared to the solid heat balance (eq. A7) and variations in inlet conditions.

The gas bulk mass balance is given by:

$$0 = \left( V_{k,0} \frac{dc_{i,k,0}}{dt} \right) = F_{tot} (y_{i,k-1,0} - y_{i,k,0}) - \Gamma_{i,k,0} (c_{i,k,0} - c_{i,k,1}) \quad (A1)$$

and the washcoat mass balance is given by:

$$0 = \left( V_{k,n} \varepsilon \frac{dc_{i,k,n}}{dt} \right) = \Gamma_{i,k,n-1} (c_{i,k,n-1} - c_{i,k,n}) - \Gamma_{i,k,n} (c_{i,k,n} - c_{i,k,n+1}) + \sum_j v_{i,j} r_{j,k,n} A_{m,k,n} \quad (A2)$$

for  $n \geq 1$

where  $r_{j,k,n}$  is the reaction rate in mole/m<sup>2</sup>Pt/s and  $A_{m,k,n}$  is the catalyst active surface area in channel segment k and wall layer n,  $V_{k,n}$  is the volume of channel segment k and layer n and  $\varepsilon$  is the washcoat porosity. Index k indicates the segment number where k=1 represents the first segment in the direction of the flow and k=K represents the last. The index n indicates the layer number where n=1 represents the first washcoat layer closest to the gas bulk, n=N represents the last layer and n=0 represents the gas bulk. The index i indicates the species.

The mass transfer coefficients  $\Gamma_{i,k,n}$  are given by:

$$\Gamma_{i,k,0} = \frac{A_k}{\frac{1}{k_{c,i,k}} + \frac{0.5\Delta x_1}{D_{eff,i,k}}} \quad (A3)$$

$$\Gamma_{i,k,n} = \frac{D_{eff,i,k} A_k}{0.5\Delta x_n + 0.5\Delta x_{n+1}} \quad (A4)$$

for  $n=1 \dots N-1$ . And for  $n = N$  it is:

$$\Gamma_{i,k,N} = 0 \quad (A5)$$

where  $A_k$  is the radial mass and heat transfer area in channel segment k. For simplicity,  $A_k$  was assumed to be constant for all wall layers.  $D_{eff,i,k}$  is the effective pore diffusion coefficient of component i in channel segment k,  $k_{c,i,k}$  is the film transfer coefficient of component i in channel segment k and  $\Delta x_n$  is the thickness of washcoat layer n.

The gas energy balance is given by:

$$0 = \left( V_{k,0} c_{p,g} \frac{dT_{g,k}}{dt} \right) = F_{tot} c_{p,g} (T_{g,k-1} - T_{g,k}) - h_k A_k (T_{g,k} - T_{s,k}) \quad (A6)$$

where  $c_{p,g}$  is the heat capacity for the gas,  $h_k$  is the heat transfer coefficient in channel segment k,  $T_{g,k}$  and  $T_{s,k}$  are the temperatures in channel segment k in the gas bulk and of the catalyst respectively. Note that the solid temperature,  $T_{s,k}$ , was not discretized radially since the high solid conductivity and short conduction distance will result in very small radial temperature gradients. The main temperature transport resistance is in other words assumed to be in the film. The solid energy balance is given by:

$$\frac{dT_{s,k}}{dt} \left( c_{p,s} m_{s,k} + \frac{s_{heat}}{K} \right) = h_k A_k (T_{g,k} - T_{s,k}) - A_s (q_{k+1} - q_k) + \sum_n \sum_j r_{j,k,n} A_{m,k,n} (-\Delta H_j) - \frac{\alpha_{tot}}{K} (T_{s,k} - T_{\infty}) \quad (A7)$$

where  $m_{s,k}$  is the mass of catalyst material and substrate in channel segment  $k$ ,  $c_{p,s}$  is the mass weighted average of washcoat and substrate heat capacity,  $A_s$  is the channel cross sectional area of the substrate and washcoat,  $\Delta H_j$  is the heat of reaction  $j$ .  $s_{heat}$  is a heat sink originating from solid material not included in the catalyst (e.g. catalyst canning and insulation). The heat loss to the environment is modeled by the lumped heat transfer parameter  $\alpha_{tot}$  and the effective environmental temperature  $T_{\infty}$ .  $K$  is the total number of channel segments.

The solid axial heat flux was calculated as:

$$q_k = -\lambda_s \frac{T_{s,k} - T_{s,k-1}}{0,5\Delta z_k + 0,5\Delta z_{k-1}} \quad (A8)$$

for  $k=2 \dots K-1, K$

$$q_k = 0 \quad (A9)$$

for  $k=1, k=K+1$

where  $\lambda_s$  is the heat conductivity for the solid material (same conductivity assumed for the washcoat and the cordierite support) and  $\Delta z_k$  is the length of channel segment  $k$  (the total heat transfer distance is half the distance of each segment).

The mass and heat transfer is described with the film model and the mass and heat transfer coefficients are given by:

$$k_{c,i,k} = \frac{Sh D_{i,k}}{d} \quad (A10)$$

$$h_k = \frac{Nu \lambda_g}{d} \quad (A11)$$

where  $D_{i,k}$  is the diffusion coefficient for component  $i$  in channel segment  $k$ ,  $\lambda_g$  is the gas heat conductivity and  $d$  is the channel dimension.  $Sh$  and  $Nu$  are the Sherwood and the Nusselt numbers respectively. Only the asymptotic values for  $Sh$  and  $Nu$  were used and thus entrance effects were neglected. Asymptotic values were taken from [35].

### Gas Diffusivity

The gas diffusivities for each component  $i$  at reference temperature ( $T_{ref}$ ) were calculated using the Fuller-Schettlet-Giddins equation [36]. Their dependence on temperature was expressed as:

$$D_{i,k} = D_{ref,i} \left( \frac{T_{s,k}}{T_{ref}} \right)^{1.75} \quad (A12)$$

The effective diffusivity for pore diffusion was initially estimated based on an additive resistance, also known as the Bosanquet formula [14]:

$$D_{eff,i,k} = \frac{f_D}{\frac{1}{D_{i,k}} + \frac{1}{DK_{i,k}}} \quad (A13)$$

Where  $f_D$  is a factor that takes into consideration the porosity and the tortuosity of the porous material.  $DK_{i,k}$  is the Knudsen diffusivity which was calculated as:

$$DK_{i,k} = \frac{d_p}{3} \sqrt{\frac{8RT_{s,k}}{\pi M_i}}$$

(A14)

where  $d_p$  is the mean pore diameter.

### Discretization

The number of segments and layers are of utmost importance for the performance of the model. A too low number of segments and layers will make the simulation dependent on the discretization and a too high number of segments and layers will lead to unnecessarily long simulation times. In this work the influence from the discretization was evaluated by gradually increasing the number of segments and layers until the change in simulated data was sufficiently low. To ensure that the selected discretization was adequate the simulation results were also compared with results from a simulation with twice the number of segments and layers. This comparison only revealed negligible differences in outlet temperature and concentrations and thus 10 segments and 8 layers was selected as the most appropriate discretization used in the current work.

A major influence on the model performance is not only the number of segments and layers but also how they are divided. In general the faster a property changes in one direction a finer discretization is needed to fully resolve a concentration or temperature gradient. For a catalyst at high temperature, the reaction rate will be high which means that some reactant components may be consumed before they have diffused radially through the washcoat. Also, the fact that diffusive flux of all components is set to zero at the washcoat-carrier material interface means that concentration gradients will approach zero close to the carrier material and be steeper at radial positions close to the surface. In other words a fine discretization close to the washcoat surface would be needed but not close to the carrier material. At low temperatures the reaction rate will be slow and concentration will not change much with radial position and thus there is little need for a fine radial discretization. With this in mind, a washcoat discretization that decreased linearly with radial position was chosen according to [equation A15](#). A result of this discretization can be observed in [figure 7](#) for eight (Mode 2 and 3) layers.

$$\Delta x_n = \left( \frac{0,02}{\sum_{i=1}^{N-1} i} (N - n) + \frac{0,98}{\sum_{i=1}^{N-1} i} (n - 1) \right) W$$

(A15)

where  $W$  is the total washcoat thickness.

For axial discretization the same way of reasoning can be applied as for radial discretization; it is more likely that the axial gradients are larger close to the inlet than close to the outlet. This indicates that a discretization decreasing with axial position would be preferable also in this direction. However, a conversion close to 100 % - which would be the case for a steep concentration gradient close to the inlet is not generally desired since these kinds of experiments are less informative in a kinetic parameter estimation point of view. With this in mind an equidistant axial discretization was selected.

## Adjustable Parameters

### Kinetic Parameters

Both the pre exponential factors,  $A_j$ , and the activation energies,  $E_{A,j}$ , can be tuned. The scaling of  $E_{A,j}$  was straightforward and performed according to

$$E_{A,j} = E_{A,j}^o + w_{Ea,j} p_{Ea,j}$$

(A16)

Where  $w$  is a weight factor for every parameter and  $p$  is the parameter that is changed by the gradient search method. The superscript "o" in the equations above indicates that this is the original values taken from literature or previous successful parameter tuning. The reaction rate coefficients were centered around a reference temperature to decrease the parameter correlation [37].

$$k_{j,ref}^o = A_j^o e^{-\frac{E_{A,j}^o}{RT_{ref}}}$$

(A17)

The reaction rate coefficient  $k_{j,ref}$  was scaled according to

$$\ln(k_{j,ref}) = \ln(k_{j,ref}^0) + w_{a,j} p_{a,j} \quad (A18)$$

The tuned rate constant at a reference temperature was then used to calculate the pre-exponential factor

$$A_j = k_{j,ref} e^{\frac{E_{A,j}}{RT_{ref}}} \quad (A19)$$

When [equation A19](#) is inserted into the expression for the reaction rate coefficient in [equation 6](#), the following expression for the tuned reaction rate coefficient is obtained

$$k_j = k_{j,ref} e^{-\left(\frac{E_{A,j}}{R} \left(\frac{1}{T_s} - \frac{1}{T_{ref}}\right)\right)} \quad (A20)$$

### Mass Transport Parameters

The mass transport was tuned by adjusting the effective diffusivities for the species taking part in the reactions.

$$f_{D_{scale,i}} = f_{D_{scale,i}}^0 + w_{D_{scale,i}} p_{D_{scale,i}} \quad (A21)$$

This will change the expression for the effective diffusivity according to

$$D_{eff,i,k} = \frac{f_D}{\frac{1}{D_{i,k}} + \frac{1}{D_{K,i,k}}} f_{D_{scale,i}} \quad (A22)$$

The value for  $f_{D_{scale,i}}^0$  is typically around 1.

### Heat Transport Parameters

The heat loss to the environment was modeled as a part of the total heat balance in [equation A7](#) and the parameters  $s_{heat}$ ,  $\alpha_{tot}$  and  $T_{\infty}$  could be adjusted. The parameter scaling and tuning was performed in the same way as the other parameters:

$$T_{\infty} = T_{\infty}^0 + w_{T_{\infty}} p_{T_{\infty}} \quad (A23)$$

$$\alpha_{tot} = \alpha_{tot}^0 + w_{\alpha_{tot}} p_{\alpha_{tot}} \quad (A24)$$

$$s_{heat} = s_{heat}^0 + w_{s_{heat}} p_{s_{heat}} \quad (A25)$$

## Erratum

Lundberg, B., Sjoblom, J., Johansson, Å., Westerberg, B. et al., "Parameter Estimation of a DOC from Engine Rig Experiments with a Discretized Catalyst Washcoat Model," *SAE Int. J. Engines* 7(2): 1093-1112; 2014, doi:10.4271/2014-01-9049

On page 1103, the published paper omitted important text before and after figure 6. The text should read as follows:

The analysis of the Weizs modulus is strictly based on simulation data and to get a confirmation of mass transfer limitations in the measurement data additional analysis is necessary. In figure 6 the temperature dependence of the conversion of NO is shown for three different transients and two catalyst configurations. The NO conversion is calculated relative to the thermodynamic limitation, which means that a 100% conversion corresponds to an outlet NO concentration equal to the thermodynamic limitation, see equation 9.

$$NO_{conv} = \frac{y_{NO,in} - y_{NO,out}}{y_{NO,in} - y_{NO,th}} \quad (9)$$

Where  $NO_{conv}$  is the NO conversion and  $y_{NO,th}$  is the thermodynamic limit for NO mole fraction calculated at outlet conditions. It should be noted that the transients in figure 6 are taken from data spanning several minutes and the influence from physisorbed NO from time points outside of the depicted data therefore should be negligible. The difference in exhaust composition and flow will however be of importance for the NO conversion which is also the main reason why the conversions differ between the three transients.

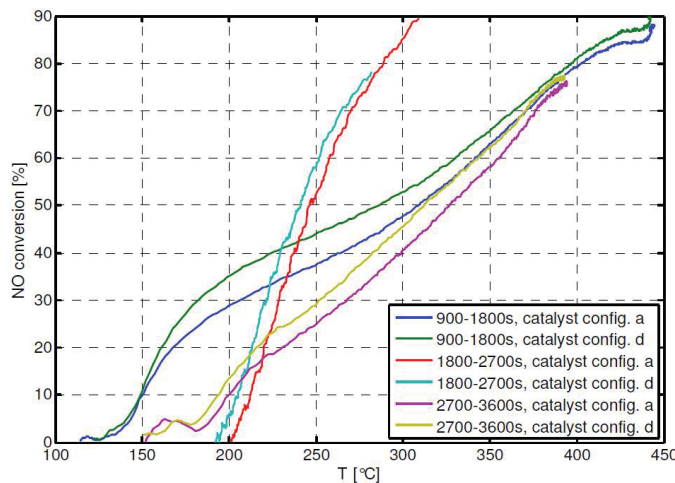


Figure 6. Comparison of NO conversion between catalyst configuration a and d at three different transients in temperature occurring between 900 s and 2700 s of the simulation shown in figure 9.

The catalyst configurations compared in figure 6 have the same amount of noble metal (15 g/ft<sup>3</sup>monolith) but different washcoat thicknesses (0.110 mm for configuration a and 0.055 mm for configuration d). The thinner washcoat of catalyst configuration d results in lower internal transport resistance than for catalyst configuration a which will give a higher conversion for catalyst configuration d if internal mass transport is present. When the three different temperature transients in figure 6 are compared it is apparent that the conversion is indeed higher for catalyst

configuration d at certain temperatures. At lower temperatures the conversion will be limited by kinetic reaction rate which means that only the platinum loading will be of influence and not the transport resistances. As the temperature increases the influence of internal transport resistance also increases which can be seen as a difference in conversion between the two catalyst configurations for all three transients at temperatures above 200 °C. This difference is most pronounced for the transients taken between 900 s and 1800 s but is also clear for the two other transients. At even higher temperatures the external mass transport resistance gets more dominant which will result in a more equal conversion for the catalyst configurations at higher temperature. The fact that the conversions are equal at low temperatures is a good indication that the difference in conversion when the temperature is increased is not attributed to a difference in dispersion but rather to internal transport resistance.

Even though measurement data indicate that there will be mass transfer limitations for catalyst configuration a for the NO oxidation reaction the Weisz-moduli presented in figure 4 are low. For example the Weisz-modulus for Mode 3 is below 0.3 at 250°C for all the transients shown in figure 6 which could indicate that the estimated effective diffusivity for NO is too high.